Dyes and Pigments 218 (2023) 111495

Contents lists available at ScienceDirect

Dyes and Pigments

journal homepage: www.elsevier.com/locate/dyepig

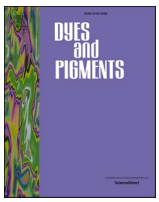

Exploring the impact of structural rigidification of amino-substituted bio-inspired flavylium dyes in DSSCs

Ana Lucia Pinto [a], Patrícia Máximo [a], João Pina [b], Giuseppe Calogero [c], César.A.T. Laia [a], A. Jorge Parola [a,*], J. Carlos Lima [a,**]

[a] LAQV-REQUIMTE, Chemistry Department, NOVA School of Science and Technology, FCT NOVA, Universidade NOVA de Lisboa, 2829-516, Caparica, Portugal
[b] CQC-IMS, Department of Chemistry, University of Coimbra, 3004-535, Coimbra, Portugal
[c] CNR, Instituto per i Processi Chimico-Fisici, Sede di Messina, Salita Sperone, C. da Papardo, I-98158, Faro Superiore, Messina, Italy

ARTICLE INFO

Keywords:
Dye-sensitized solar cells
Flavylium salts
Bio-inspired dyes
Titanium dioxide

ABSTRACT

Sharing with anthocyanins the 2-phenyl-1-benzopyrylium structural motif, flavylium derivatives are strongly colored bio-inspired dyes that have been explored in dye-sensitized solar cells (DSSCs). Following on the fact that the most efficient flavylium-based dyes for DSSCs require amine electron-donating groups, a diethylamino group and the corresponding rigidified julolidine group were introduced in the benzopyrylium core. This structural variation was combined with another structural parameter – increased planarization of the flavylium ring system – to yield four flavylium derivatives all with a catechol anchoring group. The several pK_a values of the new dyes and the UV–vis absorption data at different pH values and upon adsorption to TiO_2 (corroborated by TD-DFT calculations) demonstrate a stronger delocalization of the nitrogen lone pair in the julolidine systems when compared to the diethylamino ones, reflecting the stronger electron-donating ability of the former. However, the julolidine-based dyes resulted in a decrease in all DSSC parameters, with efficiencies of 0.6% *vs*. 2.3% for the diethylamino devices. Discarding eventual increased self-aggregation processes of the more planar julolidine derivatives through studies with a de-aggregating agent (CDCA), and determining comparable dye loadings for all dyes, the presence of increased back-electron transfer processes for the julolidine-based compounds is advanced to explain their lower efficiencies. Rigidification of the flavylium dyes by bridging the benzopyrylium and the phenyl rings is demonstrated by higher fluorescence quantum yields and by electrochemical data and leads to a slight increase in the efficiency of the respective DSSCs. The results contribute to consolidate the potential of flavylium dyes as sensitizers for DSSCs.

1. Introduction

Flavylium compounds are versatile molecules that comprise anthocyanins, the natural pigments responsible for the colors seen in a broad variety of flowers, fruits, vegetables and roots. [1] These compounds give rise to different colors (from yellow, to red, and blue) by means of structural variations depending on external *stimuli* such as pH, temperature and light. In fact, they share the same chemical equilibrium network in acid to neutral medium (Scheme 1). In the case of anthocyanins, the flavylium cation ($\mathbf{AH}^+$) is the predominant species in equilibrium under sufficiently acidic conditions. However, when amino groups are introduced in the flavylium core, $\mathbf{AH}^+$ may persist up to pH values near neutrality. [2] Once the pH is raised the flavylium cation is involved in two parallel reactions: deprotonation of phenol groups in the flavylium structure to form the blue quinoidal base (**A**) and/or hydration to form a colorless hemiketal (**B**). Since hemiketal formation occurs from the hydration of the flavylium cation and not from the quinoidal base, these two reactions are competitive. This means that **A** appears as a kinetic product, and later totally or partially disappears to yield the thermodynamic equilibrium species, forming the hemiketal through the flavylium cation. The pale yellow *cis*-chalcone (**Cc**) is formed from the hemiketal by a tautomeric process, and finally (in a longer timescale) *cis*-chalcone isomerizes and gives the *trans*-chalcone (**Ct**). [1] At equilibrium, the flavylium system can be considered equivalent to that of a single acid-base equilibrium between flavylium cation and a conjugate base (**CB**), defined as the sum of the concentrations of all the basic species in the network,

* Corresponding author.
** Corresponding author.
E-mail addresses: ajp@fct.unl.pt (A.J. Parola), lima@fct.unl.pt (J.C. Lima).

https://doi.org/10.1016/j.dyepig.2023.111495
Received 16 March 2023; Received in revised form 22 June 2023; Accepted 22 June 2023
Available online 3 July 2023

$$[\mathbf{CB}] = [\mathbf{A}] + [\mathbf{B}] + [\mathbf{Cc}] + [\mathbf{Ct}] \quad \text{(Eq. 1)}$$

$$\mathbf{AH}^+ + H_2O \overset{K_a'}{\rightarrow} \mathbf{CB} + H_3O^+ \quad \text{(Eq. 2)}$$

where,

$$K_a' = K_a + K_h + K_h K_t + K_h K_t K_i \quad \text{(Eq. 3)}$$

Until recent years, dye-sensitized solar cells (DSSCs) exhibiting high energy conversion yields were based on functional ruthenium complexes, which are expensive and toxic. [3] Since the pioneering works of Tennakone, [4] and Grätzel and co-workers, [5] where anthocyanin derivatives were used as dye-sensitizers, extensive work has been focused on sustainable DSSCs based on natural anthocyanins. [6–11] However, despite conferring to nature a variety of colors, these naturally selected structures are often not optimized for efficient electron transfer for application on DSSCs. Following a bio-inspired strategy one can prepare biomimetic compounds with the adequate structural modifications. Employing simple, non-toxic and environmentally safe synthetic procedures, it is possible to synthesize compounds with properties similar to those of natural occurring anthocyanins while tailoring desirable traits such as absorption properties, electron-donor moieties and charge transfer character. In fact, simple structural modifications of cyanidin-3-glucoside led to 7-diethylamino-3′,4′-dihydroxyflavylium which attained a conversion yield of 2.2% and, upon device assembly optimization, achieved an efficiency of 3.0%. [12,13].

Recent studies with pyranoflavylium derivatives, which belong to the anthocyanin family, have also pointed to the impact of substitution of methoxy and hydroxy groups by dimethylamine moieties, emphasizing the importance of studying stronger amine-derived donors for DSSC applications of anthocyanin-based dyes. [14] Furthermore, effective participation of the dialkylamine electron pair in charge transfer and a more rigid sensitizer chromophore were shown to be preferable in order to obtain faster electron injection, minimize energy losses and increase the overall DSSC performance, reaching efficiencies up to 2.6%, for non-optimized devices. [14] Overall, amine-based moieties showed to be promising in a D-π-A (Donor-[π--bridge]-Acceptor) molecular motif. [2,15].

Herein, following up on previous results, a series of new amino-based flavylium derivatives (compounds **2**–**4**, Scheme 2), inspired in compound 7-diethylamino-3′,4′-dihydroxyflavylium (compound **1**, Scheme 2) were developed in the context of their application as photosensitizer dyes in DSSCs. We focused on studying the impact of rigidifying the structure of the electron-donating moiety, by replacing diethylamine with a julolidine moiety in position 7 (compounds **3** and **4**). The insertion of a julolidine moiety introduces two new C–C bonds (in positions 6 and 8), which extends the dye absorbance towards the red region of the visible spectrum and potentially affects the pK_a and pK'_a values, serving as a stronger electron-donating moiety. Simultaneously, rigidification of the flavylium structure between rings C and B was also studied, in order to conclude about the impact of this structural modification in the performance of the assembled devices, *i.e.* increased efficiency from potential minimization of energy losses of the excited state through coupling to vibrational modes and/or faster electron injection. We used spectrophotometric titrations and photophysical characterization of the flavylium species as well as theoretical calculations to understand the impact of rigidifying the donor-moiety and the flavylium structure. The current *vs.* potential properties of photoanodes containing these dyes were measured and a relation was established between power conversion efficiency and dye structure. This work aims to provide insight into the influence of the introduced modifications in the overall performance of DSSCs based on these dyes, in hope to establish a precise guide to the synthetic development of new optimized bio-inspired dyes based on this family of compounds.

2. Experimental (Materials and Methods)

2.1. Synthesis

All solvents and chemicals employed for synthesis and for preparation of samples were of reagent or spectrophotometric grade and were used as received. Millipore grade water was used. Reversed phase silica gel (LiChroprep, RP-18 40–63 μm, Merck) was used for column chromatography.

NMR spectra were recorded in DMSO-d_6 with 5% (v/v) trifluoroacetic acid-D on a 400 MHz (100 MHz for ^{13}C) Brucker Avance III 400 or 500 MHz (125 MHz for ^{13}C) Bruker AVANCE Neo 500 spectrometer at 25 °C using standard pulse programs. Residual solvent signals were used for calibration (^{1}H: 2.50 ppm, ^{13}C: 39.5 ppm). High resolution mass spectra were run on an Agilent 6200 Series TOF/6500 Series Q-TOF B.06.01 (B6172 SP1) in FIA mode.

Flavylium salt 7-(*N,N*-diethylamino)-3′,4′-dihydroxyflavylium chloride (**1**) was synthesized according to a previously published procedure. [12] Compound 6,7-dihydroxytetralone was synthesized according to Liao et al.. [16].

10-(Diethylamino)-2,3-dihydroxy-5,6-didydrobenzo[*c*]xanthen-12-ium chloride (**2**) - To 229.4 mg (1.29 mmol) of 6,7-dihydroxy-1-tetralone, 170.4 mg (0.88 mmol) of 4-diethylaminosalicylaldehyde were added, and the mixture dissolved with 4 ml of glacial acetic acid and 1.0 ml of conc. H_2SO_4. The reaction was allowed to proceed overnight at 50 °C. Precipitation with diethyl ether afforded 356.6 mg (0.82 mmol, 93.2%) of the flavylium hydrogensulfate salt. Afterwards, 205.4 mg (0.47 mmol) were recrystallized from MeOH/HCl and diethyl

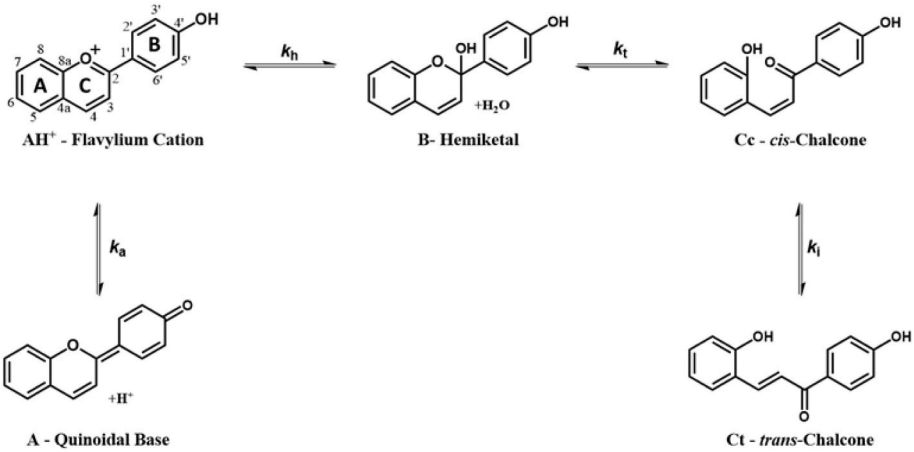

Scheme 1. Flavylium network of chemical reactions exemplified from 4′-hydroxyflavylium.

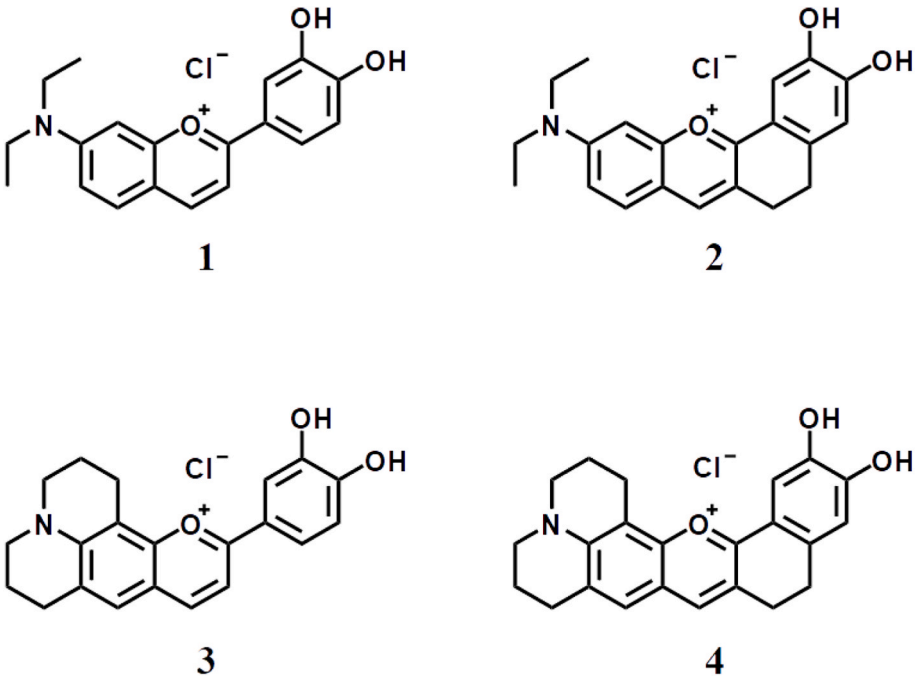

Scheme 2. Chemical structures of the four flavylium derivatives studied in this work in their cationic form.

ether. The flavylium chloride salt (53.3 mg, 0.14 mmol) was recovered leading to a global yield of 27.8%. ^{1}H NMR (400 MHz) δ: 8.58 (s, 1H), 7.89 (*d*, 9.0, 1H), 7.64 (s, 1H), 7.38 (*d*, 9.0, 1H), 7.19 (s, 1H), 6.85 (s, 1H), 3.66 (*q*, 6.8, 4H), 3.00–2.90 (m, 4H), 1.23 (*t*, 6.8, 6H). ^{13}C NMR (125 MHz) δ: 164.2, 157.6, 154.5, 154.0, 147.3, 145.7, 137.5, 131.4, 120.6, 117.4, 116.9, 116.8, 115.8, 112.4, 95.6.45.2, 25.8, 25.0, 12.4. ESI-MS (+) (*m/z*): [M+] 336.1594, calc. for $[C_{21}H_{22}NO_3]^+$ 336.1599.

11-(3,4-Dihydroxyphenyl)-2,3,6,7-tetrahydro-1*H*,5*H*-pyrano [2,3-*f*] pyrido [3,2,1-*ij*] quinolin-12-ium chloride (**3**) - To 305.1 mg (2.00 mmol) of 3′,4′-dihydroxyacetophenone, 437 mg (2.01 mmol) of 8-hydroxyjulolidine-9-carboxaldehyde were added, and the mixture dissolved with 6 ml of glacial acetic acid and 1.5 ml of conc. H_2SO_4. The reaction was allowed to proceed overnight at room temperature. Precipitation with diethyl ether afforded 436.9 mg (1.01 mmol, 50.63%) of the flavylium hydrogensulfate salt. Afterwards, 300.0 mg (0.69 mmol) were purified by reverse phase column chromatography using a gradient of H_2O/MeOH with 1% TFA. The pure flavylium (99.1 mg, 0.22 mmol) was recovered from the fraction eluted with H_2O/MeOH – 4/6. Recrystallization of 96.2 mg (0.22 mmol) from MeOH/HCl afforded 47.3 mg (0.13 mmol) of the flavylium chloride salt with a global yield of 9.5%. ^{1}H NMR (400 MHz) δ: 8.43 (*d*, 8.1, 1H), 7.74 (*d*, 8.1, 1H), 7.65 (*dd*, 8.5 and 2.1, 1H), 7.61 (*d*, 2.0, 1H), 7.52 (s, 1H), 6.98 (*d*, 8.4, 1H), 3.57–3.56 (m, 4H), 3.00–2.98 (m, 2H), 2.88–2.85 (m, 2H), 2.02–1.94 (m, 4H). ^{13}C NMR (100 MHz) δ: 164.7, 153.1, 152.1, 152.0, 146.3, 146.2, 127.9, 127.1, 121.3, 121.0, 118.0, 116.6, 113.8, 107.1, 104.5, 50.6, 50.1, 27.0, 19.8, 19.0, 18.8. ESI-MS (+) (*m/z*): [M+] 334.1438, calc. for $[C_{21}H_{20}NO_3]^+$ 334.1444.

13,14-Dihydroxy-2,3,6,7,10,11-hexahydro-1*H*,5*H*-benzo [7,8] chromeno [2,3-*f*] pyrido [3,2,1-*ij*] quinolin-16-ium chloride (**4**) - To 244.2 mg (1.37 mmol) of 6,7-dihydroxytetralone, 230.5 mg (1.06 mmol) of 8-hydroxyjulolidine-9-carboxaldehyde were added, and the mixture dissolved with 4 ml of glacial acetic acid and 1.0 ml of conc. H_2SO_4. The reaction was allowed to proceed overnight at 50 °C. Precipitation with diethyl ether afforded 363.6 mg (0.79 mmol, 74.5%) of the flavylium HSO_4^- salt. After, 199.2 mg (0.44 mmol) were recrystallized from MeOH/HCl and diethyl ether. The flavylium chloride salt (40.4 mg, 0.10 mmol) was recovered leading to a global yield of 16.9%. ^{1}H NMR (400 MHz) δ: 8.36 (s, 1H), 7.52 (s, 1H), 7.48 (s, 1H), 6.82 (s, 1H), 3.57–3.53 (m, 4H), 3.03–2.86 (m, 8H), 2.03–1.93 (m, 4H). ^{13}C NMR (125 MHz) δ: 161.9, 152.3, 150.9, 145.5, 145.4, 136.0, 127.3, 126.4, 119.2, 117.6, 117.4, 115.8, 111.4, 104.4, 50.3, 49.9, 27.0, 25.8, 24.9, 19.9, 19.0, 18.8. ESI-MS (+) (*m/z*): [M+] 360.1597, calc. for $[C_{23}H_{22}NO_3]^+$ 360.1594.

2.2. Characterization

2.2.1. Physico-chemical characterization of the compounds –

Optical measurements: The UV–Vis absorption spectra were recorded in solution using a Varian Cary 5000 Spectrometer (Santa Clara, CA, USA). The solution spectra were collected between 250 and 850 nm at room temperature, with a 1 nm interval, at full slit height, in double beam mode. The absorption spectra of the concentrated dye solutions for DSSC applications were recorded using QS-1, 1 mm path length quartz cuvettes. The absorption spectra of the dyes adsorbed onto TiO_2 were measured in a solid sample holder in transmittance mode using a Varian Cary 5000 (Santa Clara, CA, USA). The titanium oxide film employed for Vis absorption experiments was prepared by doctor blade: two edges of the conductive glass plate (area: 15 cm × 4 cm) were covered with strips of an adhesive tape (3 M Magic) and the transparent titania paste (18NR-T, Greatcell Solar, Queanbeyan, Australia) was spread uniformly on the substrate by sliding a glass rod along the tape spacer. The TiO_2-coated plates were gradually heated up to 325 °C, then the temperature was increased to 375 °C in 5 min, and afterwards to 500 °C. The plates were sintered at this temperature for 30 min, and finally cooled down to room temperature. Each slide was cut into rectangular pieces (area: 1 cm × 4 cm), resulting in slides with a transparent ultrathin TiO_2 film with an estimated thickness of about 6 μm. The TiO_2-coated slides were soaked for 1h in an ethanol solution of the dye at a concentration of 0.5 mM, at room temperature in the dark. The excess dye was removed by rinsing the photoanodes with the same solvent as that employed for the dye solution. The Vis absorption spectra of the dyes adsorbed to TiO_2 were collected between 400 and 850 nm at room temperature, with a 1 nm interval, at full slit height, in double beam mode.

The fluorescence measurements were performed on a Horiba Jobin Yvon Fluorolog FL3-22 fluorimeter, using 1 cm × 1 cm quartz cuvettes. All emission spectra were collected with 4 and 3 nm slit bandwidth for excitation and emission, respectively. All the spectra were corrected unless stated otherwise. Fluorescence quantum yields were calculated

by the relative method using optically matched solutions of Nile Blue in methanol as standard (QY = 0.27). [17].

2.2.2. Determination of pK_a values –

Stock solutions ($1x10^{-4}$ M) of the flavylium compounds were prepared in 0.1 M HCl water:ethanol 60:40 (V:V) and protected against light. The resulting low pH value of the stock solutions (pH ≈ 1) ensured that most of the compounds were in their cationic form (see Scheme 3). The thermodynamic acidity constants were determined from batch titrations involving direct pH jumps, mixing a specific amount of stock dye solution, with an equal volume of universal buffer solution [18] and enough NaOH to neutralize the initial HCl, covering the pH range between 1 and 10. After each addition, the mixture was shaken, and rapidly a UV–Vis spectrum was recorded. The pH was recorded with a Radiometer Copenhagen PHM240 pH/ion meter (pH values below 2 were calculated from the analytical concentration of H^+).

2.2.3. Differential pulse voltammetry (DPV) –

Measurements were performed on a μAutolab Type III potentiostat/galvanostat (Metrohm Autolab B. V., Utrecht, The Netherlands), controlled with GPES (General Purpose Electrochemical System) software version 4.9 (Eco-Chemie, B. V. Software, Utrecht, The Netherlands), using a cylindrical 5 mL three-electrode cell. A Pt wire was used as counter-electrode. To perform the measurements on the dye-coated TiO_2 films, the films themselves were used as working electrode. A fresh sample was used for each scan to avoid uncertainty due to degradation between scans. The electrolyte composition was 0.1 M tetrabutylammonium tetrafluoroborate (TBATFB) in acetonitrile:valeronitrile (85:15, % v/v). All potentials refer to an SCE (Saturated KCl) reference electrode (Metrohm, Utrecht, The Netherlands). DPV measurements were performed between 0 and +1 V, using a scan rate of 10 mV/s and a pulse amplitude of 50 mV. The samples in the electrochemical cell were de-aerated by purging with nitrogen for 10 min prior to, and during, the electrochemical measurements.

2.2.4. DSSCs fabrication and photovoltaic characterization –

The detailed procedure has been described elsewhere. [19] The conductive FTO-glass (TEC7, Greatcell Solar, Queanbeyan, Australia) used for the preparation of the transparent electrodes was first cleaned with detergent and then washed with water and ethanol. To prepare the anodes, the conductive glass plates (area: 15 cm × 4 cm) were immersed in a $TiCl_4$/water solution (40 mM) at 70 °C for 30 min, washed with water and ethanol and sintered at 500 °C for 30 min. This procedure is essential in order to improve the adherence of the subsequently deposited nanocrystalline layers to the glass plates, as well as to serve as a 'blocking-layer', helping to block charge recombination between electrons in the FTO and holes in the I^-/I_3^- redox couple. Afterwards, the TiO_2 nanocrystalline layers were deposited on these pre-treated FTO plates by screen-printing the transparent titania paste (18NR-T, Greatcell Solar, Queanbeyan, Australia) using a frame with polyester fibers having 43.80 mesh per cm^2. This procedure, involving two steps (coating and drying at 125 °C), was repeated twice. The TiO_2-coated plates were gradually heated up to 325 °C, then the temperature was increased to 375 °C in 5 min, and afterwards to 500 °C. The plates were sintered at this temperature for 30 min, and finally cooled down to room temperature. A second treatment with the same $TiCl_4$/water solution (40 mM) was performed, following the procedure previously described. This second $TiCl_4$ treatment is also an optimization step that enhances the surface roughness for dye adsorption, thus positively affecting the photocurrent produced by the cell under illumination. Finally, a coating of reflective titania paste (WER2-O, Greatcell Solar, Queanbeyan, Australia) was deposited by screen-printing and sintered at 500 °C. This layer of 150–200 nm sized anatase particles functions as a 'photon-trapping' layer that further improves the photocurrent. Each anode was cut into rectangular pieces (area: 2 cm × 1.5 cm) having a spot area of 0.196 cm^2 with a thickness of 15 μm. The prepared anodes were soaked for 15 h in an ethanol solution of the dye (0.5 mM), at room temperature in the dark. The excess dye was removed by rinsing the photoanodes with the same solvent as that employed for the dye solution. For the study of the impact of chenodeoxycholic acid (CDCA) addition on the photovoltaic properties of the cells, all the above adsorption process was repeated for each compound with a 0.5 mM solution of the dye prepared in ethanol with 50 mM CDCA.

Each counter-electrode consisted of an FTO-glass plate (area: 2 cm × 2 cm) in which a hole (1.5 mm diameter) was drilled. The perforated substrates were washed and cleaned with water and ethanol in order to remove any residual glass powder and organic contaminants. The transparent Pt catalyst (PT1, Greatcell Solar, Queanbeyan, Australia) was deposited on the conductive face of the FTO-glass by doctor blade: one edge of the glass plate was covered with a strip of an adhesive tape (3 M Magic) both to control the thickness of the film and to mask an electric contact strip. The Pt paste was spread uniformly on the substrate by sliding a glass rod along the tape spacer. The adhesive tape strip was removed, and the glasses heated at 550 °C for 30 min. The photoanode and the Pt counter-electrode were assembled into a sandwich type arrangement and sealed (using a thermopress) with a hot melt gasket made of Surlyn ionomer (Meltonix 1170-25, Solaronix SA, Aubonne, Switzerland). The I^-/I_3^- electrolyte was prepared by dissolving LiI (0.8 M) and I_2 (0.05 M) in an acetonitrile/valeronitrile (85:15, % v/v) mixture. The electrolyte was introduced into the cell *via* backfilling under vacuum through the hole drilled in the back of the cathode. Finally, the hole was sealed with adhesive tape.

For each compound, three to five cells were assembled under the same conditions, and the efficiencies were measured in order to calculate average and standard deviation values.

2.2.5. Photoelectrochemical measurements –

Current-Voltage curves were recorded with a digital Keithley SourceMeter multimeter (PVIV-1A) (Newport, M. T. Brandão, Porto, Portugal) connected to a PC. Simulated sunlight irradiation was provided by an Oriel solar simulator (Model LCS-100 Small Area Sol1A, 300 W Xe Arc lamp equipped with AM 1.5G filter, 100 mW cm^{-2}) (Newport, M. T. Brandão, Porto, Portugal). The external quantum efficiency (EQE) measurements were performed using a Newport QuantX-300 system, equipped with a Xenon lamp of 100 W, at wavelength intervals of 10 nm with a nominal illumination spot size of 0.8 x 1.1 mm.

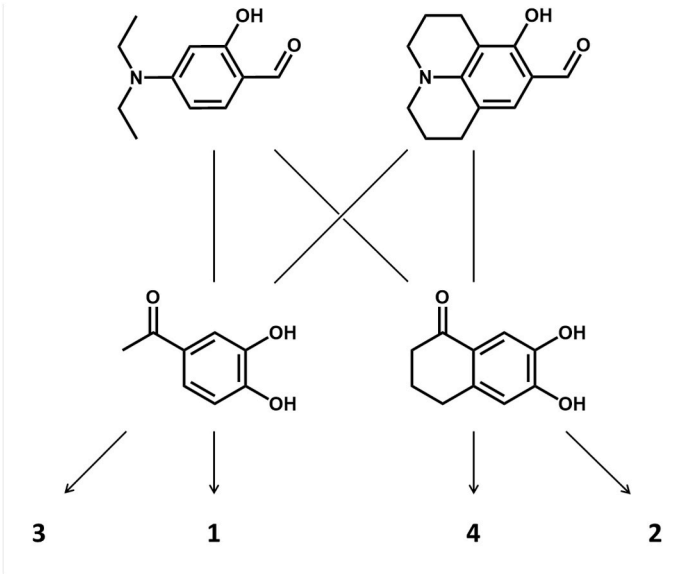

Scheme 3. Schematic representation of the synthetic approach used for compounds **1**–**4**, indicating their respective salicylaldehyde and acetophenone precursors.

The thickness of the oxide film deposited on the photoanodes and TiO_2 slides was measured using an Alpha-Step D600 Stylus Profiler (KLA-Tencor, Milpitas, CA, USA).

2.2.6. Dye loading measurements –

Dye loading estimations were made by the difference method described next: 1) the absorption spectra of the 0.5 mM fresh ethanolic solution of the dyes was measured 2) dye adsorption onto the TiO_2 photoanodes was performed by dipping the anodes in the previous solution for 15 h; 3) the absorption of the solution after the adsorption period was measured, 4) the amount of dye adsorbed was calculated from the difference in absorbance from the solutions prior to, and after, dye adsorption at 555 nm (compounds **1** and **3**), 585 nm (**2**) and 596 nm (**4**). The UV–Vis absorption spectra were recorded using a Varian Cary 5000 Spectrometer (Santa Clara, CA, USA). The spectra were collected between 250 and 850 nm at room temperature, with a 1 nm interval, at full slit height, in double beam mode. The absorption spectra of the dye solutions were recorded using QS-1, 1 mm path length quartz cuvettes.

2.2.7. Computational details –

All of the calculations were performed using Gaussian 09. [20] The geometries of the isolated flavylium dyes and the TiO_2 cluster alone in the ground state were first fully optimized by DFT calculations with the B3LYP/6-311g(d,p) method. [21,22] The starting geometry for the TiO_2 cluster in this study was taken from literature [23] and to avoid the problem of associating formal charges with the cluster a finite, neutral, stoichiometric cluster model $Ti_3O_{11}H_{10}$ was used. [24] The molecular structures were optimized without conformation restrictions and the frequency analyses was performed at the same level of theory as geometry optimizations to confirm that all optimized structures are a local minimum on the potential energy surface. For the adsorption systems dyes (quinoidal base or deprotonated quinoidal base):TiO_2, different interfaces and specific sites in the TiO_2 fragment were tested for the interface, according to the three possibilities described in literature: [25–31] the monodentate mode (the molecule bound to one Ti(IV) site *via* one of the oxygen sites of the catechol group), the bridging bidentate mode (the molecule bound to two Ti(IV) sites *via* the two oxygen sites of the catechol group) and the chelating bidentate mode (the molecule bound to one Ti(IV) site *via* the two oxygen sites of the catechol group), see Fig. S1 in Supporting Information with the representative structures for dye **1**:TiO_2. Deprotonation of the flavylium OH substituents of the catechol group was considered for all the systems, making Ti–O molecular bonds which is preferred to molecular adsorption. [26] The geometry of the cluster was frozen throughout all the calculations, but the structure of the adsorbed dyes was optimized. The calculated vertical electronic excitation energies for the monodentate mode with the molecule bound to the peripheral Ti(IV) site demonstrated to better predict the optical absorption spectra of the studied compounds adsorbed on a TiO_2 thin film. The absorption spectra were predicted by time dependent DFT (TD-DFT) [32,33] calculations at the B3LYP/6-311g(d,p) level (wavelength, oscillator strength and active molecular orbitals with their highest contributions percentage, see Table S1) using the polarizable continuum model (PCM) [34] to account for the solvation effects of acetonitrile, which is generally used in the fabrication of DSSCs. The calculated UV–Vis spectra were plotted using GAUSSUM 2.2 program [35] and the molecular orbital contours were plotted using GaussView 6 program (see Figs. S2 and S3).

3. Results and discussion

3.1. Synthesis

The synthesis of flavylium compounds was carried out through the acid-catalysed condensation of acetophenones with salicylaldehydes. Aiming to combine the effects of rigidification on the two points responsible for conformational freedom along the path for electron transfer from the amine to TiO_2 (see Scheme 2): (i) rotation around the N–C bond connecting the amine to the 2-phenyl-benzopyrylium moiety (compounds **1** and **3** in Scheme 2) and (ii) rotation around the C–C bond connecting the benzopyrylium to the phenyl ring (compounds **2** and **4** in Scheme 2), syntheses were performed combining a free and a rigidified acetophenone, with a free and a rigidified salicylaldehyde, as depicted in Scheme 3. The chemical structures of the newly synthesized compounds were confirmed by NMR and high-resolution mass spectroscopy (see Figs. S4–S12).

3.2. Determination of pK_a values

The flavylium derivatives were fully characterized with respect to their pK_a and pK'_a values. The network of chemical reactions was studied by UV–Vis spectrophotometry from direct pH jumps. pH jumps are a convenient way to study the flavylium-based multistate systems, through addition of base to a solution of the flavylium cation stabilized at a pH low enough to have $\mathbf{AH}^+$ as the sole species, in most cases at pH 1. A direct pH jump triggers a series of spontaneous chemical reactions through a complex succession of kinetic processes occurring in different timescales. [2] Herein, the multistate system of the compounds was studied by batch titrations involving direct pH jumps from stock solutions of the compounds in 0.1 M HCl. The absorption spectra of each compound were obtained for the pH range between 1 and 10, 30 s after direct pH jumps. The flavylium multistate system and the related spectroscopic changes are quite relevant in the context of the application of this family of compounds in DSSCs, as previously discussed. [14] Upon increasing the pH, there are observable changes in the absorption spectrum that impact light absorption by the dye. Additionally, there is a change in the protonation degree that affects the dye's performance as an electron-donor. [14] When the absorption spectra are taken right after the pH jump, the variations are compatible with an acid-base equilibrium between $\mathbf{AH}^+$ and **A**. In the case of polyprotic compounds, the global sequential deprotonation process (Scheme 4) can be accounted for by eqs. (S1)-(S2) [see Supporting Information].

The inspection of the results for compound **2** in Fig. 1 shows the potential existence of two acid-base equilibria (pK_{a2} and pK_{a3} in Scheme 4). Since the acidity constants are sufficiently different, isosbestic points can be observed in restricted pH ranges (see Fig. 1a and b) and the mathematical fit of the absorption data was consistent with two pK_a values (Fig. 1c). At the starting acidic pH, the predominant species is the flavylium cation. The increase of pH from 1.0 to 5.5 (Fig. 1a), leads to the disappearance of the flavylium cation with the concomitant formation of a new species, exhibiting a red-shifted absorption band, which can be attributed to the highly conjugated quinoidal base (see Scheme 4). The calculated $pK_{a2} = 5.2$ is assigned to the deprotonation of the 4′-hydroxy substituent in ring B, as observed in many analogous flavylium cation derivatives. [12,36] Upon further increase in pH (Fig. 1b), $pK_{a3} = 9.2$ is calculated and should correspond to deprotonation of the last hydroxyl substituent. The amine in position 7 can only be protonated in extremely acidic solutions (HCl 12 M) (Fig. S13) ($pK_{a1} \approx -0.4$). Nitrogen protonation leads to loss of conjugation, resulting in a blue-shift of the spectra, leading to the yellowish color of the $\mathbf{AH_2^{2+}}$ species, as observed for other amino-based flavylium derivatives. [12,36].

Identical studies were performed for compounds **1**, **3** and **4** (see Supporting Information, Figs. S14–S20), and the respective pK_a values are collected in Table 1.

Inspection of Table 1 reveals important information about the donor ability of the studied dyes. Comparing the results for compounds **1** *vs.* **3** and **2** *vs.* **4**, it is evident that the latter have significantly higher pK_{a2} values, which can be attributed to the decrease in conformational freedom of the amine in the julolidine-based compounds, **3** and **4**, that should increase the planarity and consequent participation of the nitrogen lone pair in the π system, increasing its electron donation. [2] Furthermore, the values for pK_{a1} corroborate this interpretation, since compounds **3** and **4**, with a julolidine moiety, present the lowest pK_{a1}

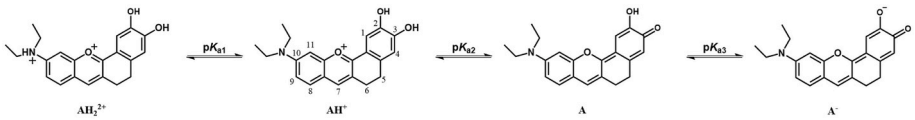

Scheme 4. Network of chemical reactions for flavylium **2** in aqueous solution after pH jump.

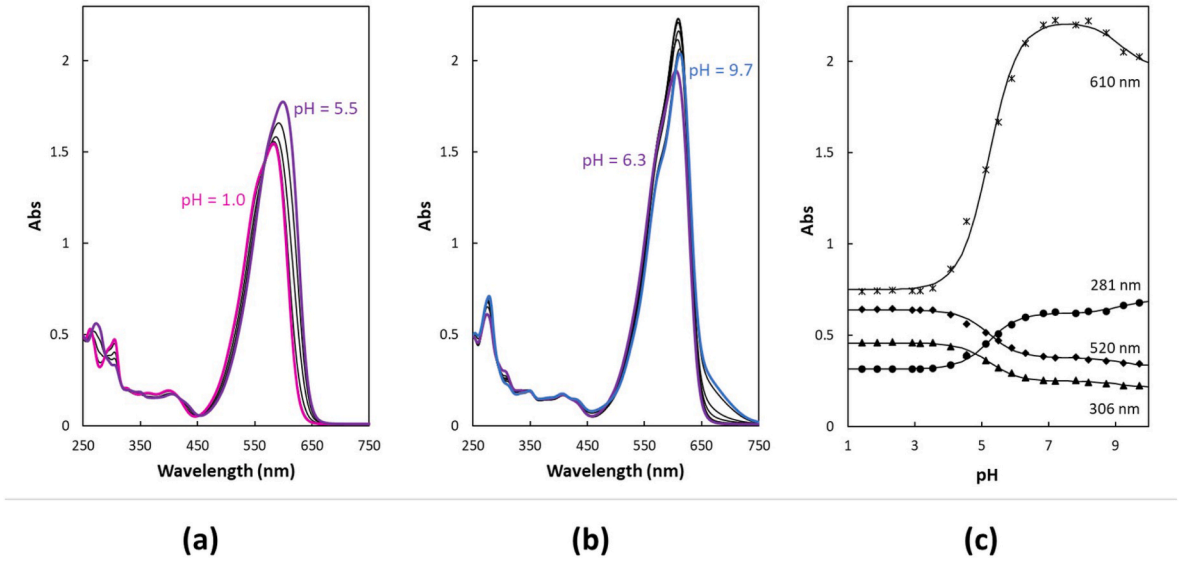

Fig. 1. pH dependent spectral variations of compound **2** in water:ethanol (60:40, % v/v) solution after direct pH jumps: a) 1.0 < pH < 5.5; b) 6.3 < pH < 9.7; c) pK_a fits: pK_{a2} = 5.2; pK_{a3} = 9.2. The colors depicted in the spectra approximately represent the colors seen in the solutions at the studied concentrations.

Table 1
Protonation constants of the compounds studied in this work in water:ethanol (60:40, % v/v) solutions.

Compound	pK_{a1} [a]	pK_{a2}	pK_{a3}	pK'_a
1	−0.8	6.1	>9	4.8
2	−0.4	5.2	9.2	5.1
3	< −1.0	6.4	8.3	6.5
4	−0.9	6.1	>10	5.7

[a] protonation constants determined by adding 0.25 mL of the dye stock solution in water:ethanol (60:40, % v/v) to 0.75 mL of HCl solutions.

values, reflecting that they are less available to protonation. For compound **4** (Fig. S16), in concentrated HCl solution (12 M), the protonated flavylium cation is predominant, but a small contribution of the non-protonated flavylium cation is still present, whereas for compound **2** (Fig. S13) a complete protonation is observed. This result is even more striking for compound **3** (Fig. S15), which even in a 12 M HCl solution presents a large contribution of the flavylium cation. In fact, the overall acidity constants (pK'_a) also indicate that the julolidine moiety is a stronger electron-donor than diethylamine. The higher pK'_a constants verified for compounds **3** and **4** indicate an increased participation of the amine electrons in charge transfer to the benzopyrylium ring, rendering the nucleophilic hydration process less favorable. [1] These results emphasize the idea that, a stronger electron donor ability of the lone pair of the amine occurs in the rigidified structure, restricted to a conformation that maximizes the overlap between the orbital of the nitrogen containing the lone pair and the π orbital of the aromatic system. [2].

3.3. Optical properties

The UV–Vis absorption and fluorescence emission spectra of the compounds were measured at room temperature in water:ethanol (60:40, % v/v) solutions at three significant pH values, where different species are present (see Fig. 2 for pH 1 and Fig. S21 for pH 7 and 10).

All compounds display strong visible light absorption, a crucial requirement for dye sensitizers to be exploited in DSSCs. Both amine and flavylium rigidification resulted in an increase in charge transfer, as seen by the resulting red-shift in the absorption and emission spectra. Furthermore, flavylium rigidification between rings C and B resulted in a significant increase in molar absorptivity (see Table 2), from 27375 to 40920 $cm^{-1}M^{-1}$ for diethylamine derivatives, and from 23592 to 32019 $cm^{-1}M^{-1}$ for julolidine derivatives. However, amine rigidification, *i.e.*, replacing diethylamine by julolidine, resulted in the opposite effect, suggesting slightly higher π–π* character in the case of diethylamine (less participation of the non-bonding electron pair in the optical transition). Rigidifying the flavylium structure also resulted in an increase in the fluorescence emission intensity. Specially at pH 7, where the quinoidal base is the dominant species, the rigidification results in a noticeable increase in fluorescence quantum yield when comparing compounds **1** *vs.* **2** and **3** *vs.* **4** (see Table 2). This can be attributed to the fact that, in the excited state, the rotation around the bond between rings C and B is an important dissipative channel for non-radiative decay in the non-rigidified compounds. Hence, non-rigidified structures as in **1** and **3**, can freely rotate, resulting in a decrease in emission, whereas rigidified structures, as **2** and **4**, see their emission properties enhanced by this restriction.

It is important to refer that, while at pH 1 only one species is present in solution (the flavylium cation), the increase in pH, to pH 7 and pH 10, leads to a fluorescence signal with contributions of **A** and $\mathbf{A}^-$ forms, where the excitation spectra, indicate a contribution of more than one species. This result is more evident for compounds **1** and **3**, the compounds with a more flexible structure.

One interesting aspect to notice is that at pH 7 the fluorescence quantum yield of compounds **1** and **2** (diethylamine derivatives) are lower than those of their julolidine counterparts **3** and **4**, leading to the conclusion that the free rotation of the amine is also an important non-radiative channel for excited state deactivation. These results can

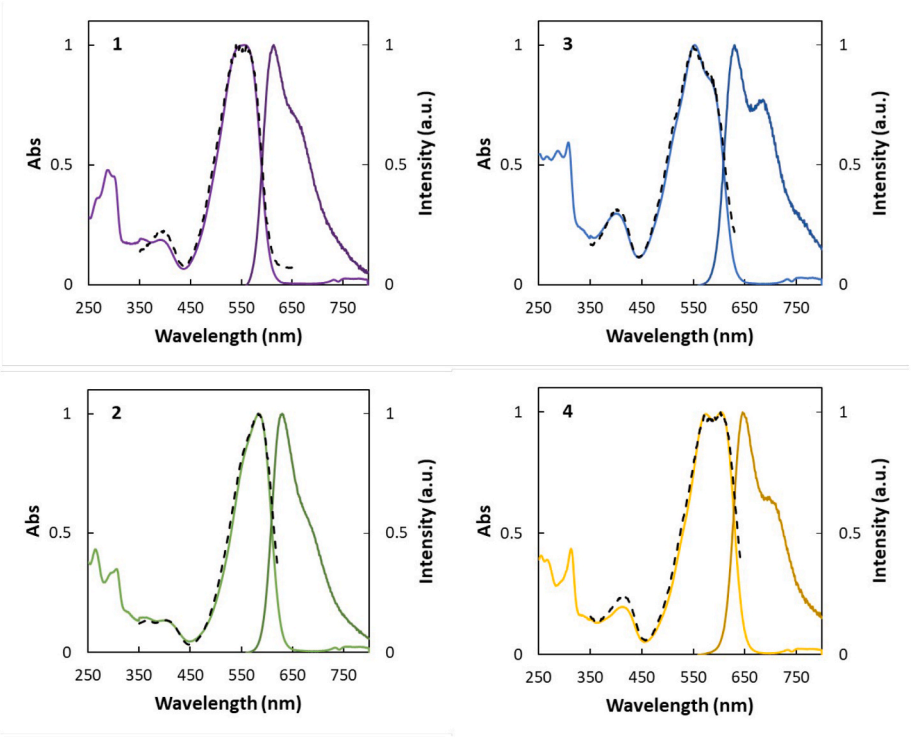

Fig. 2. Normalized absorption and fluorescence emission spectra for the studied compounds in water:ethanol (60:40, % v/v) solutions at pH 1; λ_{exc} = 550 nm. Excitation spectra depicted in black dashed line; λ_{em} (**1**) = 675 nm, λ_{em} (**2**) = 630 nm, λ_{em} (**3**) = 640 nm, λ_{em} (**4**) = 650 nm.

Table 2
Spectroscopic data for the studied compounds in water:ethanol (60:40, % v/v) solutions (absorption and fluorescence emission maxima, fluorescence quantum yield, Φ_f, molar extinction coefficients, ε, and Stokes shift, Δ_{SS}) at room temperature. Fluorescence reference: Nile Blue in methanol.

Compound	pH	λ_{max}^{Abs} (nm)	λ_{max}^{Fluo} (nm)	Φ_f (%)	ε (cm^{-1} M^{-1})	Δ_{SS} (cm^{-1})
1	1	556	614	4.7	27375	1699
	7	592	632	0.5	–	1069
	10	611	641	0.2	–	766
2	1	583	630	14.0	40920	1280
	7	612	643	11.2	–	788
	10	614	644	5.7	–	759
3	1	553	630	3.5	23592	1076
	7	606	638	4.4	–	828
	10	611	643	1.3	–	815
4	1	604	646	5.0	32019	1076
	7	626	658	19.7	–	777
	10	629	659	9.6	–	724

indicate the presence of non-radiative twisted-intramolecular charge transfer states for diethylamino derivatives, which are absent in julolidine derivatives, thus presenting a higher fluorescence quantum yield.

3.4. Optical and electrochemical properties of the adsorbed dyes

In order to establish a relation between dye structure (and the electron donor ability) and cell performance, a complete study of the dye-TiO_2 complexation was made. Dye adsorption was performed from 0.5 mM ethanolic solutions. The solutions are mainly composed of flavylium cation with a small contribution of the quinoidal base species as reflected in the respective absorption spectra (Fig. 3a). Upon dye adsorption an evident broadening of the bands is verified, accompanied by the appearance of small shoulders in the longer wavelength region of the spectra, which is an indication of adsorption *via* quinoidal base (**A**) and/or deprotonated quinoidal base ($\mathbf{A}^-$) (Fig. 3b). Coordination to Ti (IV) *via* a quinoidal base (**A**) or its deprotonated form ($\mathbf{A}^-$) usually results in a red-shift of the absorption maximum. The interaction of flavylium cations with some metal ions such as aluminum(III), iron(III) and titanium(IV), is known to involve deprotonations and formation of metal complexes with the deprotonated quinoidal bases, displacing the equilibrium toward the complexing deprotonated quinoidal form. [5,37–39] Moreover, the appearance of a new broadened charge transfer band in the absorption spectra upon adsorption, with respect to that of the free dyes, points to the occurrence of a one-step electron injection from the ground state of the dyes to the conduction band of the semiconductor upon photoabsorption (type II photoinjection mechanism). [40].

Differential pulse voltammetry (DPV) was used to electrochemically characterize the dye-TiO_2 complex (Fig. 4). The inspection of Fig. 4 for compounds **1** and **3** reveals the presence of a lower current intensity oxidation wave, starting around 0.1 V. These waves can be attributed to the oxidation of the catechol moiety in ring B for conformers in which ring B is decoupled from the rest of the molecule (probably twisted). The free rotation between rings C and B for these two compounds is thought to lead to a small contribution of molecules with different torsion angles between the abovementioned rings, justifying the absence of this first oxidation peak for compounds **2** and **4**. Given that these oxidation waves result from the contribution of only a small fraction of molecules, for compounds **1** and **3,** the onset was calculated from the anodic oxidation waves presenting higher current intensity values.

To ensure efficient electron injection, an important thermodynamic requirement in DSSCs is that electron transfer from the excited state of the dye to TiO_2 must be faster than the decay to the ground state. The LUMO of the dye should be sufficiently high in energy for efficient charge injection into the TiO_2 conduction band (−4.24 eV). [41] Also, the HOMO level of the sensitizer must be sufficiently low in energy for efficient regeneration of the oxidized dye by the redox couple. [42] To experimentally determine the HOMO and LUMO energy levels of the compounds, the first oxidation and reduction potentials obtained from voltammetry experiments may, respectively, be used. Alternatively, the LUMO energy can be obtained by adding the optical absorption energy

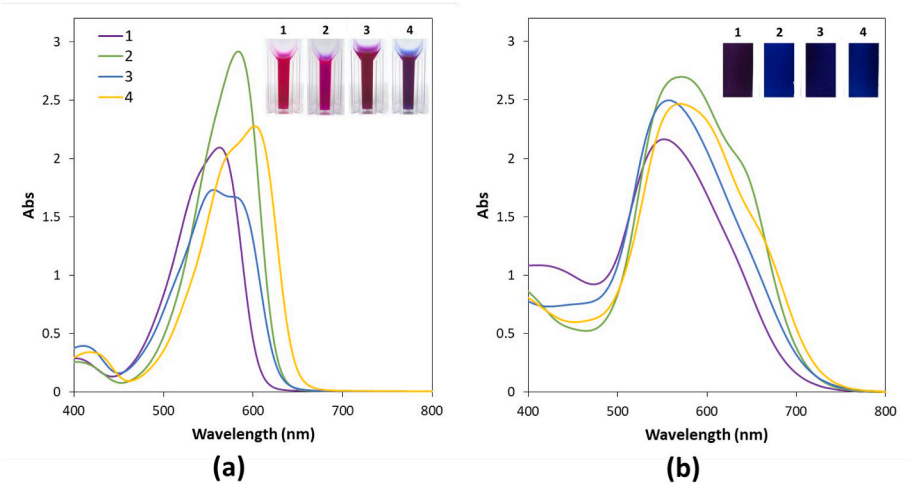

Fig. 3. UV–Vis absorption spectra of the studied compounds in (a) 0.5 mM ethanolic solution and (b) adsorbed on a TiO_2 thin film (ca. 6 μm). Insets: pictures of the solutions and colored films.

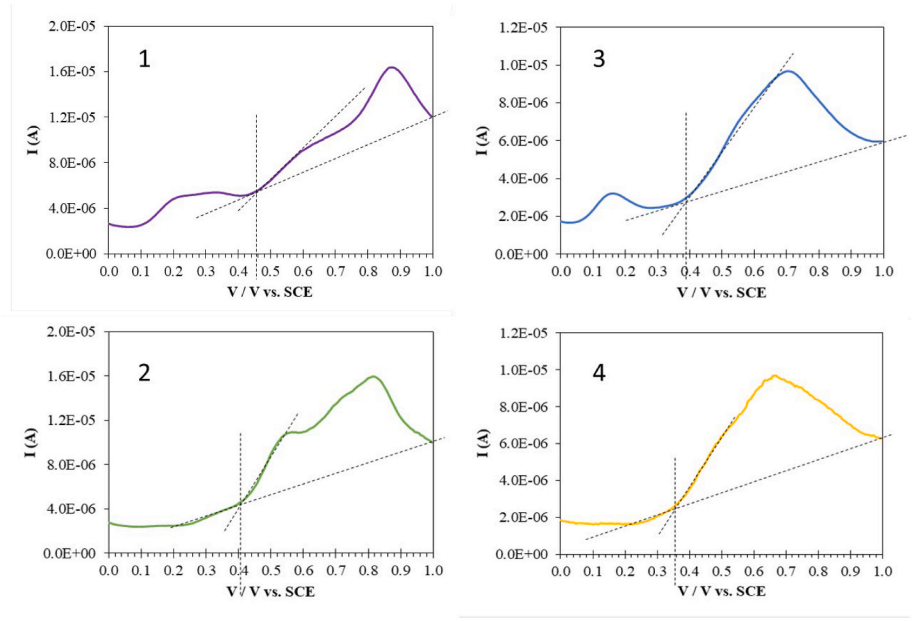

Fig. 4. DPV voltammograms (*E* vs. SCE) of compounds **1**−**4** adsorbed on a thin (*ca.* 6 μm) TiO_2 film screen-printed on FTO glass, plus 0.1 M TBATFB in ACN:VN (85:15, % v/v) in the dark. Acquisition parameters: scan rate 10 mV s^{-1} and pulse amplitude of 50 mV. The dashed lines indicate the guidelines used to define the onset value.

to the HOMO value. In here, we considered the onset of the anodic oxidation wave obtained from DPV performed on the dyes adsorbed on TiO_2, hence determining the HOMO of the dye-TiO_2 complex ($HOMO_{dye@TiO2}$) (Eq. (4)). [43] The LUMO energy for the dye-TiO_2 complex ($LUMO_{dye@TiO2}$) was obtained by adding the optical absorption energy of the TiO_2 adsorbed dyes to the respective HOMO value (Eq. (5)). These results are presented in Table 3.

$$E(HOMO_{dye@TiO2}) = -(E_{onset}\ (vs.\ SCE) + 4.44) \quad (4)$$

$$E(LUMO_{dye@TiO2}) = E(HOMO_{dye@TiO2}) + E_{absorption\ edge} \quad (5)$$

To discuss efficient electron injection processes, these HOMO and LUMO energies should be confronted with the calculated redox potential of the redox couple I^-/I_3^- (−4.72 eV) [44] and the Fermi level potential

Table 3
HOMO and LUMO energy levels of the dye-TiO_2 complex calculated from optical and electrochemical data. The absorption edge was taken as 10% of the absorption spectra of the compounds adsorbed on a TiO_2 thin film.

Compound	Absorption edge (nm)	Energy (eV)	$HOMO_{dye@TiO2}$ *vs.* SCE (V)	$HOMO_{dye@TiO2}$ *vs.* Vacuum (eV)	$LUMO_{dye@TiO2}$ *vs.* Vacuum (eV)
1	696	1.782	0.46	−4.90	−3.12
2	710	1.746	0.40	−4.84	−3.09
3	709	1.749	0.39	−4.83	−3.08
4	723	1.715	0.36	−4.80	−3.08

of the FTO (−4.4 eV), respectively. All the studied flavylium dye-TiO_2 complexes present similar HOMO and LUMO energy levels. Based solely on the inspection of the LUMO energy levels, the ability to inject electrons into the FTO band should be approximately equal for all the compounds. In the case of the HOMO level, although all the compounds possess a HOMO energy level below the potential of I^-/I_3^-, thus being able to be reduced by the electrolyte, for most of the compounds this difference is quite small (~0.1 eV). This fact can result in inefficient regeneration of the compound by the electrolyte, affecting the performance of the cell. Since the anodic waves obtained in the DPV measurements are not reversible, calculation of the HOMO energy was performed using the onset of the oxidation peak. [45] This fact resulted in less negative HOMO values. However, if we were to consider E_{pa}, or, if the peaks were reversible, $E_{1/2}$, more negative HOMO values would be obtained, increasing the difference between HOMO and the redox potential of I^-/I_3^-, resulting in an increased driving force for dye regeneration. Therefore, these calculated values (Table 3) should be viewed with caution and considered as an 'upper-limit value' for the HOMO of these compounds. As so, regeneration of all the compounds by the electrolyte can be considered efficient, thus resulting in well-functioning devices.

3.5. Photovoltaic performance of the DSSCs

The photocurrent density *vs.* voltage plots for DSSCs assembled with the flavylium dyes are shown in Fig. 5. Analysis of these data allowed determination of the short circuit current density (J_{SC}), open circuit voltage (V_{OC}), fill factor (FF) and overall conversion efficiency (η), summarized in Table 4.

The photovoltage generated by the cell under illumination corresponds to the difference between the Fermi level of the electron in the semiconductor and the redox potential of the electrolyte. [46] Therefore, the electrolyte composition used is known to have a direct impact on the V_{OC} values obtained. In here, the V_{OC} and FF values obtained are generally rather low, which can be attributed to the high lithium content of the electrolyte used. Lithium is known to act as a TiO_2 Fermi level

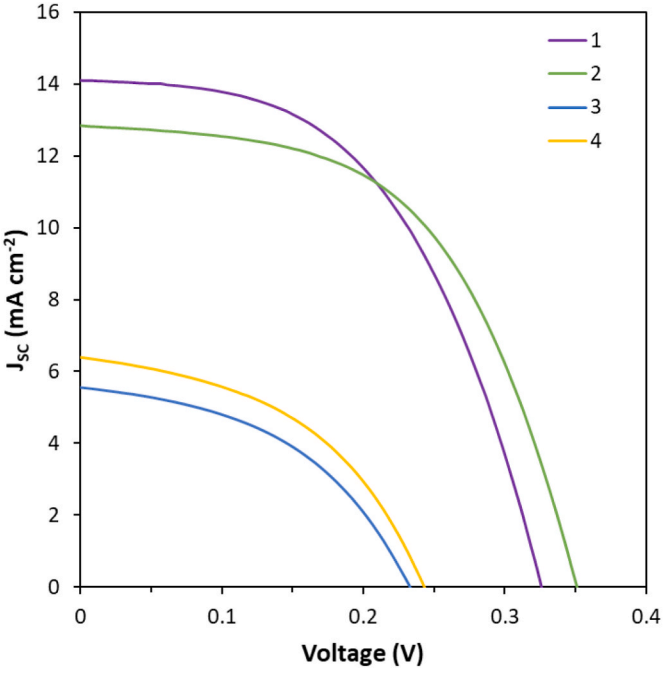

Fig. 5. *J-V* curves based on compounds **1**−**4** adsorbed from 0.5 mM ethanolic solutions measured under 100 mW cm^{-2} simulated AM 1.5G illumination, using 0.8 M LiI and 0.05 M I_2 in ACN:VN (85:15, % v/v) as electrolyte. The presented results correspond to the best performing device.

Table 4
Photovoltaic performance under 100 mW cm^{-2} simulated AM 1.5G illumination for DSSCs based on the studied compounds adsorbed from 0.5 mM solutions in ethanol. The presented results correspond to the average values of three identical, non-optimized, devices.

Compound	V_{OC} (mV)	J_{SC} (mA cm^{-2})	FF	η (%)
1	333 ± 8	13.4 ± 0.6	0.49 ± 0.02	2.2 ± 0.2
2	357 ± 8	11.8 ± 0.5	0.54 ± 0.02	2.3 ± 0.1
3	245 ± 1	5.1 ± 0.3	0.43 ± 0.02	0.54 ± 0.03
4	255 ± 1	5.9 ± 0.3	0.44 ± 0.02	0.66 ± 0.04

stabilizer, thus moving the TiO_2 conduction band towards more positive potentials, usually resulting in higher J_{SC} values in detriment of V_{OC} results. [47] Furthermore, the lack of TiO_2 surface passivation agents, such as *tert*-butylpyridine, might lead to increased recombination losses, negatively affecting both V_{OC} and FF. As previously shown, the addition of pyridine derivatives in flavylium-based DSSCs, despite resulting in higher V_{OC} values, shows a tremendous negative impact in the J_{SC} produced by the devices, resulting in *ca.* 10-fold decrease in efficiency. [19] For this reason, no pyridine derivatives were herein used.

Inspection of Table 4 shows the results seem to have a direct relation with the compounds' structure. Compounds **1** and **2**, with the diethylamine donor moiety, display the highest efficiency results (2.2 and 2.3%, respectively). Both compounds, despite the flavylium rigidification on going from **1** to **2**, show similar V_{OC} and J_{SC} results. Compounds **3** and **4** also show similar results between them, with efficiencies of 0.54 and 0.66%, respectively. Which leads to the conclusion that, despite the small increase verified in efficiency, rigidifying the flavylium structure does not result in significant performance improvements. Amine rigidification, however, showed a tremendous impact in cell performance, as seen by comparing compounds **1** *vs.* **3** and **2** *vs.* **4**. Both J_{SC} and V_{OC} decrease significantly upon amine rigidification through the julolidine moiety. Compound **1** shows a J_{SC} of 13.4 mA cm^{-2}, which is *ca.* three times higher than that displayed by **3**, 5.1 mA cm^{-2}, and a V_{OC} *ca.* 90 mV higher. Compound **2** displays twice the J_{SC} of **4** (11.8 *vs.* 5.9 mA cm^{-2}, respectively), and a V_{OC} *ca.* 100 mV higher. Despite the accumulated evidence of better electron-donating properties, with impact in acidity and hydration constants and also in the red-shift of the fluorescence emission band, julolidine substitution in compounds **3** and **4** resulted in a decrease of *ca.* 4 and 3.5 times, respectively, in the efficiency of the cell. These differences are not accounted by a lower dye loading. Dye loading values were calculated from the differences in absorbance of the loading solution prior to, and after, dye adsorption onto the TiO_2 photoanodes (Table 5). The loadings seem to be reasonably similar for all compounds, thus indicating that the high discrepancy in photocurrent production is not dependent on the amount of dye adsorbed.

The photoaction spectra reported in Fig. 6 show that all compounds cover a broad range of wavelengths. In fact, the IPCEs recorded show a good overlap with the absorption spectra collected for the dyes adsorbed onto TiO_2 (Fig. S22), which proves that all wavelengths are contributing for current production. However, a closer inspection reveals that current production between 400 and 490 nm is higher than expected for all compounds. Which can be an indication that injection from lower excited states is somehow hindered, decreasing current production from higher wavelengths. Despite possessing a julolidine moiety, which is a stronger electron-donor, and thus having more red-shifted absorption, compounds **3** and **4** show low conversion values, around half the

Table 5
Estimated amount of dye loaded onto the TiO_2 photoanodes.

Compound	Dye loading (mol cm^{-2}) × 10^{-7}
1	4.5
2	5.7
3	4.4
4	2.4

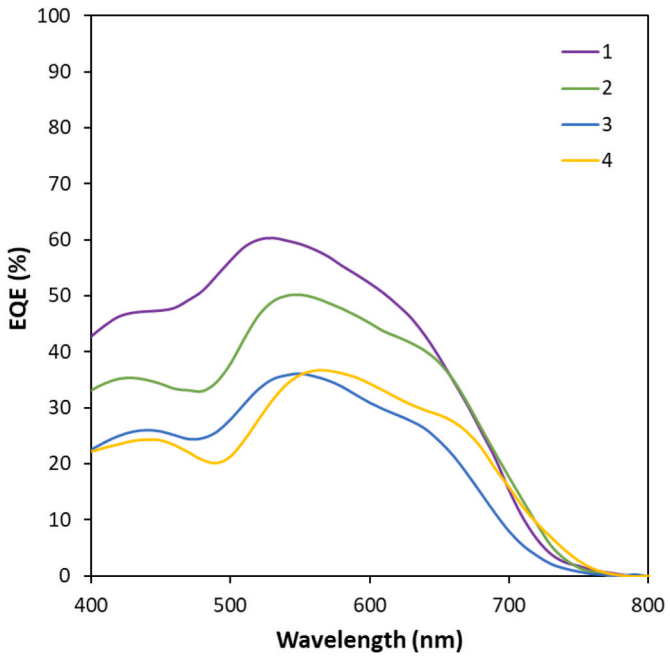

Fig. 6. IPCE spectra of the studied compounds. The results presented correspond to the best performing device.

response of **1**. The lower/inefficient electron injection ability for julolidine-derived compounds could result from the presence of aggregates or be due to quenching at the TiO_2 surface.

3.5.1. Effect of CDCA addition on the photovoltaic properties

The insertion of a julolidine moiety will render the molecules more planar, with a potentially increased tendency to form aggregates. In order to assess if the low efficiency results obtained are due to aggregates formation, studies with chenodeoxycholic acid (CDCA), a known de-aggregating agent, were performed. The use of CDCA as co-adsorber in DSSCs is known to enhance the performance of the cell, which affects the photocurrent by means of increasing charge collection and/or electron injection, and improves open-circuit photovoltage by suppressing charge recombination. [48] Furthermore, with anthocyanins, CDCA has proved to be an effective approach to avoid anthocyanins self-association, which might lead to a decrease in performance due to molecular stacking causing intermolecular energy quenching. [7,48] Herein, 50 mM of CDCA were added to the dye solutions prior to adsorption, and the results are portrayed in Table 6 and Fig. S23.

Upon CDCA addition, for compounds **1** and **2**, a clear increase in V_{OC} was verified (from 333 to 357 to 416 and 401 mV, respectively). This result is probably due to reduced dark current as a result of TiO_2 surface coverage by CDCA. Therefore, CDCA addition resulted in the desired increase in the overall efficiency of the devices, particularly for compound **1**. The lower J_{SC} results verified for all the compounds can probably be attributed to reduced dye loading, since the amount of adsorbed sensitizer is strongly dependent on CDCA presence, as confirmed by the absorption spectra (Fig. S24). All devices show an increase in FF, which can be attributed to a decrease in dark current. For julolidine derivatives, however, this increase in FF did not translate in improved efficiencies. Despite the lack of direct proportionality between the verified decrease in absorbance and the decrease in cell parameters, contrarily to the diethylamine-based derivatives, compounds **3** and **4** show a decrease in V_{OC} as well as in J_{SC} parameters.

The photoaction spectra (Fig. S25) reveal, once more, that all compounds cover a broad range of wavelengths, showing the same overall qualitative behavior, and presenting a good overlap with the absorption spectra collected for the dyes adsorbed onto TiO_2 (see Fig. 3). Despite this, the great discrepancy in the obtained results between compounds with diethylamine *vs.* julolidine was still verified. Compounds **1** and **2** show an improvement in the overall cell efficiency, while compounds **3** and **4** show a decrease in efficiency. These results led to the conclusion that the differences seen between electron-donor moieties are not due to aggregates formation, nor greatly increased dark current for julolidine derivatives, but must arise from a specific characteristic of the donor moieties.

3.5.2. Electron injection vs. electron recombination

The predicted vertical transitions and relevant molecular orbitals for the deprotonated quinoidal base species of compounds **1**–**4** anchored to a $Ti_3O_{10}H_9$ cluster (see Fig. S1 for the structure relative to dye **1**) were calculated in acetonitrile and the results are summarized in Table 7 and Table S1.

In general, the lowest energy transition presents a predominant HOMO → LUMO character, whose energy values are located between 619 and 660 nm, which could be assigned to the lowest energy band feature experimentally observed in the IPCE measurements (Fig. 6). This assignment is qualitative since the model of a dye bound to a $Ti_3O_{10}H_9$ cluster does not reproduce the reality of a dye adsorbed to a TiO_2 nanoparticle on the DSSC interface. Inspection of the molecular orbitals involved (Fig. 7) shows that the lowest energy transition presents a charge transfer character (corroborating the occurrence of a type II photoinjection mechanism), where the HOMO is located in the dye and the LUMO is located in the $Ti_3O_{10}H_9$ cluster. No significant differences are observed that could explain the different photocurrent values

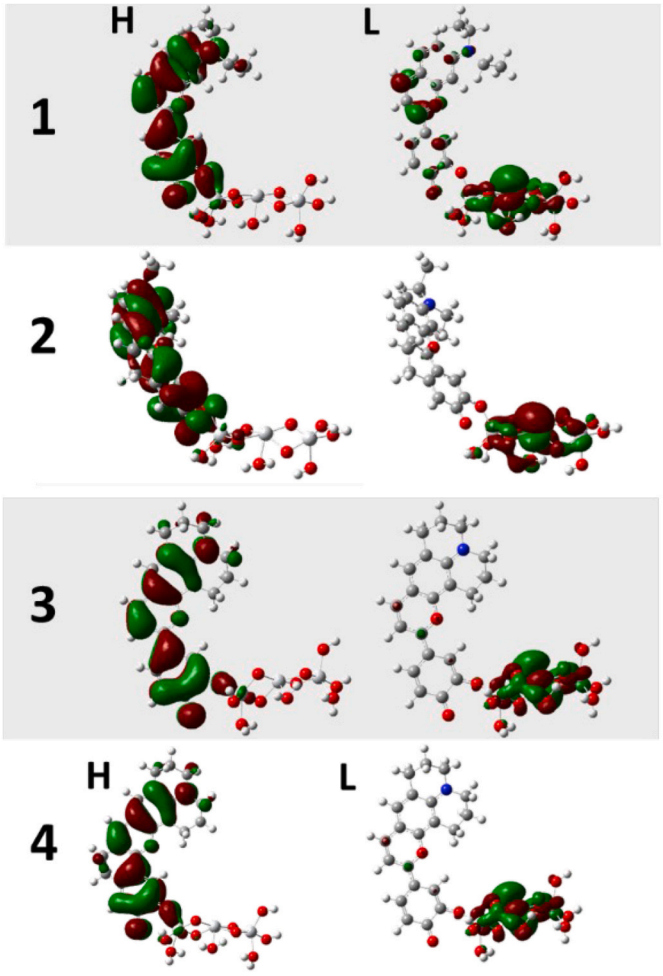

Fig. 7. Frontier molecular orbitals of the studied compounds bound to a $Ti_3O_{10}H_9$ cluster taking in consideration solvent effects (acetonitrile).

Table 6
Photovoltaic performance under 100 mW cm^{-2} simulated AM 1.5G illumination for DSSCs based on the studied compounds adsorbed from 0.5 mM solutions in ethanol plus 50 mM chenodeoxycholic acid (CDCA). The results presented correspond to the average values of three identical devices.

Compound	V_{OC} (mV)	J_{SC} (mA cm^{-2})	FF	η (%)
1 + **CDCA**	416 ± 9	11.7 ± 0.2	0.58 ± 0.01	2.82 ± 0.05
2 + **CDCA**	401 ± 7	10.7 ± 0.3	0.57 ± 0.01	2.5 ± 0.1
3 + **CDCA**	237 ± 10	3.5 ± 0.2	0.45 ± 0.02	0.37 ± 0.04
4 + **CDCA**	257 ± 11	4.3 ± 0.2	0.47 ± 0.02	0.52 ± 0.03

Table 7
Calculated wavelength (λ, nm) and active molecular orbitals, MO, with their respective highest contributions (%) for the vertical excitations of the lowest energy absorption band from TD-DFT for the studied compounds bound to a $Ti_3O_{10}H_9$ cluster, taking in consideration solvent effects (acetonitrile).

Compound	λ (nm)	Active MO major contribution (%)
1	619	HOMO → LUMO (92%)
2	619	HOMO → LUMO (98%)
3	638	HOMO → LUMO (99%)
4	660	HOMO → LUMO (98%)

experimentally verified, *i.e.*, from the point of view of electron injection the dyes should qualitatively present at least similar performances. Therefore, another dark mechanism must be considered to account for the lower performances of **3** and **4** with respect to **1** and **2**.

One possible explanation is the presence of increased back-electron transfer (BET) in the case of julolidine derivatives **3** and **4**. It was previously verified that the presence of two different emission states, intramolecular charge transfer and twisted intramolecular charge transfer (TICT), can affect the DSSC performance. [49–51] Since in the case of julolidine the positive charge resulting from charge injection is more displaced over the whole molecule, recombination with the electron injected into the TiO_2 can eventually occur, resulting in increased BET phenomena. In the case of compounds with diethylamine, holes are more localized on the nitrogen atom of the diethylamino group, leading to a much larger spatial charge separation. [49] Thus, in these devices, the presence of the julolidine moiety might be reducing electron injection and/or drastically increasing back-electron transfer. In this case, despite being a better electron-donor, the recombination processes greatly compete with electron injection into the semiconductor, decreasing the overall efficiency of the devices.

4. Conclusions

In the present work, following a bio-inspired strategy, three new amino-based flavylium compounds (**2**–**4**) were designed, synthesized and applied for the first time in DSSCs.

The pK_a determination studies pointed to an increased participation of the amine electrons in charge transfer to the benzopyrylium ring upon julolidine insertion. These results were corroborated by the optical properties of the compounds and confirmed that the substitution of diethylamine by a julolidine moiety, resulted in molecules with improved electron-donating ability. However, despite being a better electron-donating moiety, the insertion of julolidine resulted in a decrease in all cell parameters, and, consequently, in the overall cell performance. These results seemed to point to lower/inefficient electron injection ability for julolidine-based compounds. The possibility of these results being due to increased self-aggregation processes, in the case of the more planar julolidine derivatives, was discarded by the realization of studies with a de-aggregating agent (CDCA).

One possible explanation is the presence of increased back-electron transfer processes for the julolidine-based compounds. Previous studies comparing two coumarin derivatives containing diethylamine and julolidine, respectively, showed that the compound with the diethylamine moiety displayed higher electron injection and slower back-electron transfer, when compared to the latter. This was attributed to the existence of a twisted-intramolecular charge transfer state in the diethylamine derivative, which was absent in the julolidine-based one. [49] A similar scenario may be the case for the compounds studied herein. In fact, the presence of TICT states was previously verified in these family of compounds, for a dimethylamino-based pyranoflavylium. [52] A closer inspection of the fluorescence results seems to support this. The free rotation of the diethylamino moieties would be responsible for the deactivation of the excited state and, thus, the low fluorescence of the diethylamino derivatives. As shown for these compounds, at pH 7, a decrease in the fluorescence quantum yield was verified for the diethylamine-based compounds, when compared with their julolidine counterparts. This can be an indication of the presence of non-radiative intramolecular charge transfer states for the diethylamine derivatives, which are absent in julolidine derivatives, thus presenting a higher fluorescence quantum yield.

Overall, insertion of stronger electron-donating moieties is a path to continue following, consistently studying the impact on all the photochemical and photophysical properties of the compounds. Flavylium structure rigidification, despite resulting in a small increase in efficiency, was shown to be a possible means of further improving cell performance. The present work consolidates the potential of flavylium dyes as sensitizers for energy applications, while also proving the importance of systematically studying structural modifications. It takes us one step further in the quest towards the improvement of these bio-inspired molecules, in order to establish them as viable competitors for environmentally friendly solar devices.

CRediT authorship contribution statement

Ana Lucia Pinto: synthesized the compounds under the guidance of, made the spectroscopic and electrochemical characterisation, assembled and characterised experimentally the DSSCs using the techniques reported in the manuscript under the guidance of, prepared a draft of the manuscript. **Patrícia Máximo:** synthesized the compounds under the guidance of. **João Pina:** carried out the theoretical calculations. **Giuseppe Calogero:** made the spectroscopic and electrochemical characterisation, assembled and characterised experimentally the DSSCs using the techniques reported in the manuscript under the guidance of. **César. A.T. Laia:** made the spectroscopic and electrochemical characterisation, assembled and characterised experimentally the DSSCs using the techniques reported in the manuscript under the guidance of. **A. Jorge Parola:** synthesized the compounds under the guidance of, made the spectroscopic and electrochemical characterisation, assembled and characterised experimentally the DSSCs using the techniques reported in the manuscript under the guidance of, write the final manuscript. **J. Carlos Lima:** made the spectroscopic and electrochemical characterisation, assembled and characterised experimentally the DSSCs using the techniques reported in the manuscript under the guidance of, write the final manuscript, The results were discussed and the manuscript revised by all authors.

Declaration of competing interest

The authors declare that they have no known competing financial interests or personal relationships that could have appeared to influence the work reported in this paper.

Data availability

Data will be made available on request.

Acknowledgements

FCT/MCTES is acknowledged for financial support through the

Associate Laboratory for Green Chemistry-LAQV (UIDB/50006/2020 and UIDP/50006/2020), grant PD/BD/135087/2017 (ALP), and CQC-IMS through project UIDB/00313/2020 and UIDP/QUI/00313/2020. The authors acknowledge Hugo Cruz for his support with DPV measurements, and Tiago Mateus for his support with IPCE measurements.

Appendix A. Supplementary data

Supplementary data to this article can be found online at https://doi.org/10.1016/j.dyepig.2023.111495.

References

[1] Pina F, Melo MJ, Laia CAT, Parola AJ, Lima JC. Chemistry and applications of flavylium compounds: a handful of colours. Chem Soc Rev 2012;41:869–908.
[2] Avó J, Petrov V, Basílio N, Jorge Parola A, Pina F. Evidence against the twisted intramolecular charge transfer (TICT) model in 7-aminoflavylium derivatives. Dyes Pigments 2016;135:86–93.
[3] Grätzel M. Recent advances in sensitized mesoscopic solar cells. Acc Chem Res 2009;42:1788–98.
[4] Tennakone K, Kumarasinghe AR, Kumara GRRA, Wijayantha KGU, Sirimanne PM. Nanoporous TiO2 photoanode sensitized with the flower pigment cyanidin. J Photochem Photobiol Chem 1997;108:193–5.
[5] Cherepy NJ, Smestad GP, Grätzel M, Zhang JZ. Ultrafast electron injection: implications for a photoelectrochemical cell utilizing an anthocyanin dye-sensitized TiO 2 nanocrystalline electrode. J Phys Chem B 1997;101:9342–51.
[6] Hug H, Bader M, Mair P, Glatzel T. Biophotovoltaics: natural pigments in dye-sensitized solar cells. Appl Energy 2014;115:216–25.
[7] Kimura Y, et al. Characterization of dye-sensitized solar cells using five pure anthocyanidin 3-O-glucosides possessing different chromophores. J Photochem Photobiol Chem 2017;335:230–8.
[8] Mohiuddin O, Obaidullah M, Sabah C. Improvement in dye sensitized solar cells from past to present. Opt Quant Electron 2018;50:377.
[9] Güzel E, et al. Photovoltaic performance and photostability of anthocyanins, isoquinoline alkaloids and betalains as natural sensitizers for DSSCs. Sol Energy 2018;173:34–41.
[10] Calogero G, et al. Absorption spectra, thermal analysis, photoelectrochemical characterization and stability test of vegetable-based dye-sensitized solar cells. Opt Mater 2019;88:24–9.
[11] Bartolotta A, Calogero G. Dye-sensitized solar cells: from synthetic dyes to natural pigments. In: *Solar Cells and light management* 107–161. Elsevier; 2020. https://doi.org/10.1016/B978-0-08-102762-2.00004-5.
[12] Calogero G, et al. Synthetic analogues of anthocyanins as sensitizers for dye-sensitized solar cells. Photochem Photobiol Sci 2013;12:883.
[13] Calogero G, et al. Electronic and charge transfer properties of bio-inspired flavylium ions for applications in {TiO}2-based dye-sensitized solar cells. Photochem Photobiol Sci 2017;16:1400–14.
[14] Pinto AL, et al. Dye-sensitized solar cells based on dimethylamino-π-bridge-pyranoanthocyanin dyes. Sol Energy 2020;206:188–99.
[15] Mahmood A. Triphenylamine based dyes for dye sensitized solar cells: a review. Sol Energy 2016;123:127–44.
[16] Liao S-R, et al. 12-N-Methylated 5,6-dihydrobenzo[c]acridine derivatives: a new class of highly selective ligands for c-myc G-quadruplex DNA. Eur J Med Chem 2012;53:52–63.
[17] Sens R, Drexhage KH. Fluorescence quantum yield of oxazine and carbazine laser dyes. J Lumin 1981;24–25:709–12.
[18] Küster FW, Thiel A. Tabelle per le analisi chimiche e chimico-fisiche. Hoepli; 1999.
[19] Pinto AL, et al. Study of the multi-equilibria of red wine colorants pyranoanthocyanins and evaluation of their potential in dye-sensitized solar cells. Sol Energy 2019;191:100–8.
[20] Frisch MJ, et al. Gaussian 09, revision A.02. 2016.
[21] Becke AD. A new mixing of Hartree–Fock and local density-functional theories. J Chem Phys 1993;98:1372–7.
[22] Francl MM, et al. Self-consistent molecular orbital methods. XXIII. A polarization-type basis set for second-row elements. J Chem Phys 1982;77:3654–65.
[23] Kılıç M, Çınar Z. A quantum mechanical approach to TiO2 photocatalysis. J Adv Oxid Technol 2009;12.
[24] Bredow T, Pacchioni G. A quantum-chemical study of Pd atoms and dimers supported on TiO2(110) and their interaction with CO. Surf Sci 1999;426:106–22.
[25] Coppola C, et al. In silico investigation of catechol-based sensitizers for type II dye sensitized solar cells (DSSCs). Inorg Chim Acta 2021;518:120233.
[26] Luppi E, Urdaneta I, Calatayud M. Photoactivity of molecule–TiO 2 clusters with time-dependent density-functional theory. J Phys Chem A 2016;120:5115–24.
[27] Syres KL, et al. Adsorbate-induced modification of surface electronic structure: pyrocatechol adsorption on the anatase TiO 2 (101) and rutile TiO 2 (110) surfaces. J Phys Chem C 2012;116:23515–25.
[28] Saiz-Poseu J, Mancebo-Aracil J, Nador F, Busqué F, Ruiz-Molina D. The chemistry behind catechol-based adhesion. Angew Chem Int Ed 2019;58:696–714.
[29] Finkelstein-Shapiro D, et al. Direct evidence of chelated geometry of catechol on TiO 2 by a combined solid-state NMR and DFT study. J Phys Chem C 2016;120:23625–30.
[30] Negre CFA, Fuertes VC, Oviedo MB, Oliva FY, Sánchez CG. Quantum dynamics of light-induced charge injection in a model dye-nanoparticle complex. J Phys Chem C 2012;116:14748–53.
[31] Liu LM, Li SC, Cheng H, Diebold U, Selloni A. Growth and organization of an organic molecular monolayer on TiO 2: catechol on anatase (101). J Am Chem Soc 2011;133:7816–23.
[32] CASIDA ME. Time-dependent density functional response theory for molecules. 1995. p. 155–92. https://doi.org/10.1142/9789812830586_0005.
[33] Gross EKU, Kohn W. Time-dependent density-functional theory. 1990. p. 255–91. https://doi.org/10.1016/S0065-3276(08)60600-0.
[34] Hamad S, Catlow CRA, Woodley SM, Lago S, Mejías JA. Structure and stability of small TiO 2 nanoparticles. J Phys Chem B 2005;109:15741–8.
[35] O'boyle NM, Tenderholt AL, Langner KM. cclib: a library for package-independent computational chemistry algorithms. J Comput Chem 2008;29:839–45.
[36] Moncada MC, et al. Multistate properties of 7-(N,N-diethylamino)-4′-hydroxyflavylium. An example of an unidirectional reaction cycle driven by pH. Org Biomol Chem 2004;2:2802–8.
[37] Goto T, Kondo T. Structure and molecular stacking of anthocyanins—flower color variation. Angew Chem Int Ed Engl 1991;30:17–33.
[38] Bayer E, Egeter H, Fink A, Nether K, Wegmann K. Complex Formation and flower colors. Angew Chem Int Ed Engl 1966;5:791–8.
[39] Yoshida K, Mori M, Kondo T. Blue flower color development by anthocyanins: from chemical structure to cell physiology. Nat Prod Rep 2009;26:884–915.
[40] Oviedo MB, et al. Quantum dynamical simulations as a tool for predicting photoinjection mechanisms in dye-sensitized TiO 2 solar cells. J Phys Chem Lett 2012;3:2548–55.
[41] Grätzel M. Photoelectrochemical cells. Nature 2001;414:338–44.
[42] O'Regan B, Grätzel M. A low-cost, high-efficiency solar cell based on dye-sensitized colloidal TiO2 films. Nature 1991;353:737–40.
[43] Bonomo M, et al. New pyran-based molecules as both n- and p-type sensitizers in semi-transparent Dye Sensitized Solar Cells. Dyes Pigments 2020;175:108140.
[44] Pinto AL, et al. Catechol versus carboxyl linkage impact on DSSC performance of synthetic pyranoflavylium salts. Dyes Pigments 2019;170:107577.
[45] Cardona CM, Li W, Kaifer AE, Stockdale D, Bazan GC. Electrochemical considerations for determining absolute frontier orbital energy levels of conjugated polymers for solar cell applications. Adv Mater 2011;23:2367–71.
[46] Grätzel M. Solar energy conversion by dye-sensitized photovoltaic cells. Inorg Chem 2005;44:6841–51.
[47] Jennings JR, Wang Q. Influence of lithium ion concentration on electron injection, transport, and recombination in dye-sensitized solar cells. J Phys Chem C 2010;114:1715–24.
[48] Chien C-Y, Hsu B-D. Optimization of the dye-sensitized solar cell with anthocyanin as photosensitizer. Sol Energy 2013;98:203–11.
[49] Debnath T, et al. Extensive reduction in back electron transfer in twisted intramolecular charge-transfer (TICT) coumarin-dye-sensitized TiO 2 nanoparticles/film: a femtosecond transient absorption study. Chem Eur J 2014;20:3510–9.
[50] El-Zohry AM, Karlsson M. Gigantic relevance of twisted intramolecular charge transfer for organic dyes used in solar cells. J Phys Chem C 2018;122:23998–4003.
[51] Chen K-F, et al. Photophysical studies of dipolar organic dyes that feature a 1,3-cyclohexadiene conjugated linkage: the implication of a twisted intramolecular charge-transfer state on the efficiency of dye-sensitized solar cells. Chem Eur J 2010;16:12873–82.
[52] Siddique F, et al. The electronic transitions of analogs of red wine pyranoanthocyanin pigments. Photochem Photobiol Sci 2019;18:45–53.